Laser Hole Boring into Overdense Plasma and Relativistic Electron Currents for Fast Ignition of ICF Targets

A. Pukhov* and J. Meyer-ter-Vehn

Max-Planck-Institut für Quantenoptik, Hans-Kopfermann-Strasse 1, 85748 Garching, Germany

(Received 28 April 1997)

Laser hole boring and relativistic electron transport into plasma of 10 times critical density is studied by means of 2D particle-in-cell simulation. At intensities of $I_0\lambda^2 = 10^{20}\ \mathrm{W\,cm^{-2}}\,\mu\mathrm{m}^2$, a channel 12λ deep and 3λ in diameter has formed after 200 laser cycles. The laser driven electron current carries up to 40% of the incident laser power. When penetrating the overdense region, it breaks up into several filaments at early times, but is channeled into a single magnetized jet later on. These features are essential for fast ignition of targets for inertial confinement fusion (ICF). [S0031-9007(97)04145-8]

PACS numbers: 52.40.Nk, 52.65.Rr

The concept of fast ignition of inertial confinement fusion (ICF) targets with lasers [1] involves hole boring into overdense plasma and the generation of relativistic electrons that heat the ignition spot in the precompressed fuel core. Such external ignition may strongly relax driver requirements for ICF. Still, the underlying physics is not well understood. The aim of this paper is to provide more detailed insight, based on two-dimensional (2D) particle-in-cell (PIC) simulation.

ICF targets are compressed by ablatively driven implosion on a nanosecond time scale. At ignition time, the core is surrounded by ablated plasma, falling in density from 10^5 times overcritical to critical over a distance of a few 100 μm. The ignition pulse has to drill a channel through this plasma toward the core. One expects that an energy of about 10 kJ has to be deposited within 10 ps into a 10 μg fraction of the fuel, provided it has been compressed 2000 times to 400 $\mathrm{g/cm^3}$ [2]. This implies a power of 10^{15} W for the heating pulse. Such petawatt powers have been achieved recently with chirped pulse amplification (CPA) lasers [3].

Notice that the final transport of this power to the core is by relativistic electrons, forming a current of 200 MA, if carried by 5 MeV electrons. This corresponds to 1000 times the Alfvén limit. Certainly, such a current cannot be transported as a simple beam, but it involves collective plasma transport.

Key issues discussed below include (1) the speed of ion cavitation driven by the ponderomotive force, (2) the efficiency of laser energy conversion into fast electron currents, (3) magnetic field buildup together with self-focusing of electrons and light, (4) current filamentation in the overdense region and eventual formation of a single magnetized electron jet, as well as (5) the directional stability of this jet. In these aspects, the present paper goes beyond the pioneering paper published by Wilks *et al.* in 1992 [4]. Since then, a number of experimental papers have appeared confirming (a) the onset of hole boring under the action of light pressure observing inward motion of the critical surface via redshifted reflected light [5–7], (b) the generation of hot electrons at solid surfaces by laser pulses above $10^{19}\ \mathrm{W/cm^2}$ with temperatures about 1 MeV and peaked in forward (laser) direction [8], (c) light channeling [9–12] and fast electrons [13,14] in underdense plasma, (d) the observation of x rays produced by these relativistic electrons through bremsstrahlung and K_α emission [15–17], and (e) the detection of MeV ions [18].

Electromagnetic, relativistic PIC simulations [19] provide detailed kinetic information about the laser plasma interactions. However, they demand extreme computing power and push existing computers to the very limits [20,21]. Simulating overdense plasmas, one has to resolve at least the plasma skin depth $d_p = c/\omega_p$ and the period of plasma oscillations $\tau_p = 2\pi/\omega_p$, where c is the velocity of light, $\omega_p = (4\pi e^2 n_e/m_e)^{1/2}$ is the plasma frequency, n_e is electron density, e and m_e are the charge and rest mass of the electron. For ignition configurations as described above, one finds $d_p = 1.6 \times 10^{-3}$ μm and $\tau_p = 3 \times 10^{-17}$ s. A complete simulation would need more than 10^9 particles ($10^5 \times 10^4$ cells in a 2D mesh) and 10^7 time steps, and require a year on a 1024 processor CRAY T3E. Therefore only model problems can presently be treated. Nevertheless, they provide important insight and a basis for more approximate treatment. Previous PIC simulations on laser hole boring are reported in [1,4] and on electron heating and absorption in [22–24]. Electron transport and stopping in the core are discussed in [25].

In the present 2D (x, y) simulations, light polarized in the y direction is normally incident on a plasma layer 20λ wide and 30λ thick, with uniform density $n_e/n_c = (\omega_p/\omega)^2 = 10$, where n_c is the critical density, $\omega = 2\pi c/\lambda$ the laser frequency, and λ the wavelength. As boundary conditions, we enforce constant electron and ion density at $y = \pm 10\lambda$ and allow particles to escape at the rear and also the front. Pulses have a Gaussian transverse profile of 6λ width and peak intensity I_0 in vacuum. They are semi-infinite in time and rise linearly over 20τ with $\tau = 2\pi/\omega$. The interaction physics scale

 0031-9007/97/79(14)/2686(4)$10.00

with $I_0\lambda^2$. For convenience, we set $\lambda = 1$ μm in the following, corresponding to a cycle time of $\tau = 3.3$ fs. Intensities $I_0/(10^{19}\ \mathrm{W/cm^2}) = 0.5$, 2.2, 10, and 15 are considered such that electrons are driven to relativistic energies $E_{\mathrm{kin}} = (\gamma - 1)m_e c^2$ with $\gamma = 1/(1 - \beta^2)^{1/2} \gg 1$ and $\beta = v/c$. This enhances electron mass, $m_e\gamma$, and decreases plasma frequency, $\omega_p\langle\gamma^{-1}\rangle^{1/2}$, where $\langle\cdots\rangle$ denotes a cell average. A 2D version of the PIC code VLPL (Virtual Laser Plasma Laboratory) [26] was run on 32 processors of CRAY T3D at Rechenzentrum Garching. We use a spatial mesh of 1500×1200 cells with 7×10^6 electrons and 1.8×10^6 ions. The mesh step corresponds to the Debye length at temperature $T_e = T_i = 25$ keV. The ions are protons with mass $m_i = 1836m_e$ and $Z = 1$.

The highest rate of channel boring and the most effective conversion of the laser power into the fast electrons is obtained for $I_0 = 10^{20}\ \mathrm{W/cm^2}$. The results of this simulation are shown in Fig. 1 in two columns of snapshots, taken after 330 and 660 fs. At 330 fs, the light has punched a Δ-shaped crater into the overdense plasma about 4λ in depth [Fig. 1(a-l)]. At 660 fs, it has changed its shape to a straight hole 12λ deep and 3λ in diameter [Fig. 1(a-r)]. Hole boring is driven by light pressure. It expels electrons from the interaction volume. This builds up an electric field that drags the ions. The hole boring velocity and its scaling with I_0 is found to be in fair agreement with the formula given by Wilks *et al.* [4]. Particle density and energy distributions at 660 fs are given in Figs. 2 and 3. Electron and ion densities are almost identical except for the channel center.

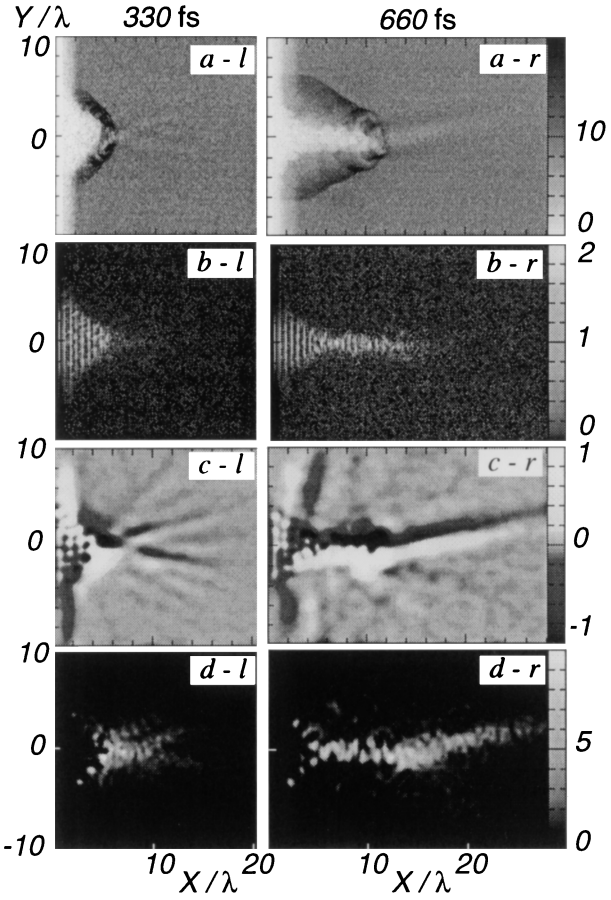

FIG. 1. Channel boring in the x, y plane by a $\lambda = 1$ μm laser pulse incident in x direction and polarized in y direction with $I_0 = 10^{20}\ \mathrm{W/cm^2}$ at times 330 fs (left column) and 660 fs (right column): (a) ion density n_i/n_c, (b) instantaneous light intensity I ($10^{20}\ \mathrm{W/cm^2}$), (c) cycle-averaged magnetic field B/B_0, and (d) x component of the electron energy flux in units of $10^{19}\ \mathrm{W/cm^2}$. Grey scales are given on the right side.

In Fig. 1(a-r), one sees a collisionless shock of conical shape corresponding to ions running outwards from the channel region. They appear in Fig. 3(a) as a hot component in the ion spectrum with $T_i = 0.5$ MeV. At the shock front, one observes a peak compression of about 1.8 times the background density which somewhat decreases toward the channel boundary and then sharply drops toward the channel core. This is best seen in Fig. 2(b). Inside the channel, the electron density is $n_e/n_c \approx 2$. Nevertheless, the laser light can propagate due to relativistically induced transparency. In order to make this evident, we have also plotted $n_e\langle\gamma^{-1}\rangle/n_c$ which indeed falls well below one. In the rest of the plasma, $n_e\langle\gamma^{-1}\rangle/n_c \approx 5$ such that the third and higher harmonics can freely propagate all over the volume.

Light intensity is plotted in Figs. 1(b) with the bright vertical lines corresponding to the wave crests. At 330 fs, the incident light just fills the crater; after 660 fs, it is funneled into the density channel, seen in Fig. 1(b-r) as a single light filament with 2λ width and 10λ length. Actually, the width of the filament oscillates, similar to

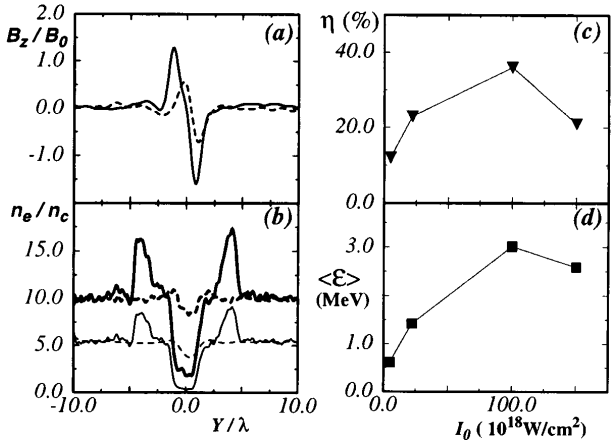

FIG. 2. Transverse profiles of (a) a cycle-averaged magnetic field and (b) an electron density cutting the light channel at $x = 7\lambda$ (solid lines), and the electron jet at $x = 16\lambda$ (dashed lines) at 660 fs. The thinner lines in (b) give $n_e\langle\gamma^{-1}\rangle/n_c$, showing the effect of relativistic mass increase. (c) Power of forward electron flow η in percent of incident laser power, and (d) average energy $\langle\varepsilon\rangle$ defined in text, both given versus incident intensity I_0 and taken at 660 fs in front of the channel head.

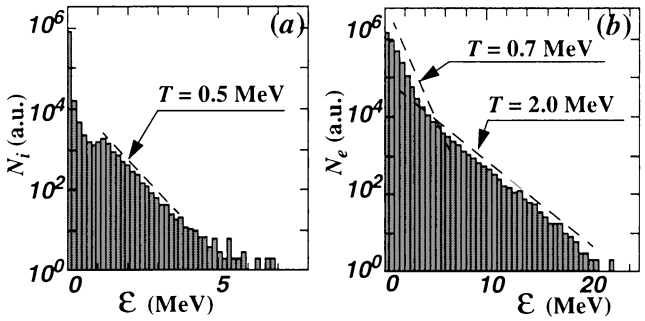

FIG. 3. (a) Ion and (b) electron distribution versus energy at 660 fs, including all particles.

what has been observed recently in underdense plasma [12]. In addition, electromagnetic energy is seen as white points scattered all over the simulation plane, more so at 660 fs. It may correspond to harmonic light and also to electromagnetic fluctuations of thermal nature, indicating plasma heating. At 660 fs, the electron energy distribution in Fig. 3(b) shows two populations with temperatures 0.7 and 2.0 MeV which are attributed to heated background plasma and laser-driven fast electrons, respectively.

The magnetic fields plotted in Figs. 1(c) give evidence for the electron currents driven by the incident light. These plots are cycle averaged in order to suppress the laser B field and to highlight the quasistationary component. We distinguish three regions. The largest field occurs in the channel (region I). It is an azimuthal field which corresponds to a strong current of relativistic electrons comoving with the laser light from left to right. It has been described before [20,27,28]. Its transverse profile at $x = 7\lambda$ is given in Fig. 2(a); the unit is $B_0 = mc\omega/e \approx 107$ MG for 1 μm light. Within the chosen x, y geometry, it corresponds to a channel current $J/J_0 = (B/B_0)L/\lambda$ per length L in the z direction with $J_0 = mc^3/e = 17$ kA. Taking $L = 2\lambda$ and $B/B_0 = 1.5$, we find $J = 3J_0 \approx 50$ kA. Apparently, it is close to the Alfvén current, defined as $J_A = J_0\langle\beta\gamma\rangle$.

Region II of the magnetic field is seen in Figs. 1(c) along the plasma surface ($x/\lambda \approx 2-3$). It corresponds to surface currents which first of all feed the channel current. It reaches values of $0.5B_0$ at 330 fs and falls to $(0.1-0.2)B_0$ at 660 fs. Currents are allowed to flow in through the sides due to the lateral boundary conditions.

Region III of the magnetic field is located to the right of the channel in the overdense part of the plasma. It appears to be the most interesting one in the context of this paper. In Fig. 1(c-l) at 330 fs, one observes a bunch of current filaments emerging like rays from the crater region, each marked by its magnetic field. The pattern corresponds to electrons accelerated by the laser field into a cone that opens to the right. The electron current penetrates the overdense plasma, where it induces a return current and breaks up into filaments due to the Weibel instability [29]. The filaments are also seen as an imprint in the ion density [see shocked region in Fig. 1(a-l)].

The pattern changes when the channel gets deeper and elongated. At 660 fs, only one strong filament is left. The azimuthal B field then traps all electrons below a certain transverse momentum in the channel. Nonetheless, they can propagate in the vicinity of the axis, where the magnetic field vanishes. Laser acceleration of these trapped electrons [30] leads eventually to a well-collimated electron beam, which is injected into the overdense plasma at the channel head. This may explain the formation of the single jet observed in Fig. 1(c-r). The jet is somewhat tilted relative to the x axis. We find that this tilt changes with time and decreases as the channel becomes longer. Obviously, the directional stability is an important issue for fast ignitor applications. From the present results, we cannot exclude that the direction may vary a bit statistically from shot to shot. The formation of filaments and the subsequent coalescence of these filaments is also discussed in [31]. In passing, we mention that the third harmonic light propagates along the jet, which acts as a waveguide [32].

An important aspect of the physics studied here is the transfer of energy flux from photons to electrons. This is highlighted in Figs. 1(d) in terms of the electron energy flux $F_x = \sum_i \varepsilon_i v_{xi}/\Delta V$. Here, we sum over all electrons in a cell and divide by its volume ΔV; v_{xi} is the electron velocity in the x direction and $\varepsilon_i = (\gamma_i - 1)mc^2$ is the electron kinetic energy. The electron energy flux reaches values up to 10^{20} W/cm^2, equal to the peak of the incident photon energy flux. Notice that F_x is strongly modulated with bunches of electrons longitudinally separated by about a laser wavelength. Inside the channel, we interpret these bunches as Brunel electrons [33] extracted from the channel wall by the E_y field of the laser wave and then accelerated by the $v_y B_z$ force in the x direction. Contrary to the energy flux distribution, the electron density distribution inside the channel shows no pronounced wave structure, i.e., we find no indication for electron acceleration by means of plasma waves.

Electron flow in the jet region close to the channel head is further analyzed in Fig. 2. Quantities are cycle averaged. The ratio of electron power per unit length in the z direction over that of incident light, $\eta = \int n v_x \varepsilon dy / \int I_L dy$, is plotted in Fig. 2(c) as a measure of the conversion efficiency. The corresponding average electron energy $\langle\varepsilon\rangle = \int n v_x \varepsilon dy / \int n v_x dy$ carrying this power is shown in Fig. 2(d). Both η and $\langle\varepsilon\rangle$ rise to peak values at $I_0 = 10^{20}$ W/cm^2 and then fall again. The decrease for $I_0 > 10^{20}$ W/cm^2 is attributed to insufficient magnetic trapping of electrons in the channel such that more energy is flowing to the sides rather than in the forward direction. At 660 fs, the maximum power residing in electrons amounts to 40% of the incident laser power and drops along the jet to 20% at the right

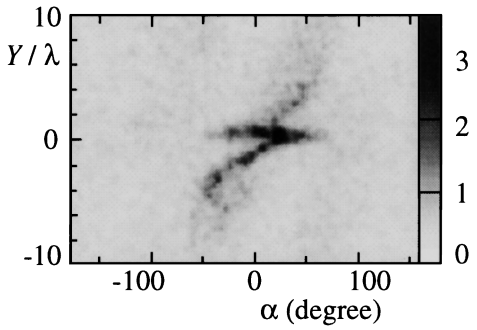

FIG. 4. Electron energy flux distribution $F(x, y, \alpha, t)$ in the y, α plane for $t = 660$ fs and $x = 16\lambda$, showing electron trapping in the magnetized jet; the angle α gives the electron direction with respect to the x axis.

boundary. The average energy $\langle\varepsilon\rangle$ is 3 MeV. From this we deduce a current density $j_B = e\eta I_0/\langle\varepsilon\rangle = 1.33 \times 10^{13}$ A/cm^2 and a beam current $J_B = 133$ kA, assuming a jet cross section of 10^{-8} cm^2. We emphasize that this beam current is much larger than the net current derived from the magnetic field. The transverse profile of the B_z field in Fig. 2(a), showing peak values of $0.6B_0$ separated by 1λ, just gives $J = 10$ kA. Apparently, J_B is strongly compensated by return currents.

The electron transport, magnetically confined to the jet, is quite different from ballistic transport. This is illustrated in Fig. 4. Here, we plot $F(x, y, \alpha, t) = \sum_i \varepsilon_i v_i/(\Delta V \Delta\alpha)$ in the y, α plane at $t = 660$ fs and $x = 16\lambda$, summing over all electrons moving within a given angle interval $\alpha \pm \Delta\alpha$ relative to the x axis. For electrons leaving the channel head with a certain angular divergence, one expects F at an upstream position x to be distributed along a sloping straight line, as partially seen in Fig. 4. Evidence for trapping in the magnetized jet is given by the horizontal bar in the distribution, representing electrons that are confined within a narrow y region (the jet), about 1λ in size, and have a large angular spread ranging between $\pm 40°$.

As to the overall energy balance at 660 fs, about 42.6% of the incident laser energy is found in the simulation volume, 33.0% in the form of electron kinetic energy, 1.5% in ions, 4.3% in electric fields, and 3.8% in magnetic fields. The residual 53.4% are in reflected light, but are also in harmonics and fast electrons that have left the simulation volume.

In conclusion, we have presented the first detailed description of laser hole boring into overdense plasma with a pulse of 10^{20} W/cm^2, based on kinetic simulation. Notwithstanding its limitations with respect to plasma density, laser spot size, as well as 2D geometry, the results reveal new features relevant to fast ignition of ICF targets, in particular, concerning generation and magnetically collimated transport of relativistic electrons with peak current densities as high as 10^{13} A/cm^2. Both current filamentation and formation of single jets should be detectable in near-term experiments. Evidently, this also opens a new field for basic plasma physics and other nonfusion applications.

This work was supported in part by BMBF (Bonn) and by EURATOM.

*Permanent address: Moscow Institute for Physics and Technology, Dolgoprudnyi, Moscow Region, Russia.

[1] M. Tabak *et al.*, Phys. Plasmas **1**, 1626 (1994).
[2] A. Caruso and V. A. Pais, Nucl. Fusion **36**, 745 (1996); S. Atzeni and M. L. Ciampi, Nucl. Fusion (to be published).
[3] M. Perry and G. Mourou, Science **264**, 917 (1994).
[4] S. C. Wilks *et al.*, Phys. Rev. Lett. **69**, 1383 (1992).
[5] M. Zepf *et al.*, Phys. Plasmas **3**, 3242 (1996).
[6] R. Kodama *et al.*, Phys. Rev. Lett. **77**, 4906 (1996).
[7] R. Sauerbrey, Phys. Plasmas **3**, 4712 (1996).
[8] G. Malka and J. L. Miquel, Phys. Rev. Lett. **77**, 75 (1996).
[9] A. B. Borisov *et al.*, Phys. Rev. Lett. **68**, 2309 (1992).
[10] P. Monot *et al.*, Phys. Rev. Lett. **74**, 2953 (1995).
[11] P. E. Young *et al.*, Phys. Rev. Lett. **75**, 1082 (1995).
[12] M. Borghesi *et al.*, Phys. Rev. Lett. **78**, 879 (1997).
[13] D. Umstadter *et al.*, Science **273**, 472 (1996).
[14] A. Modena *et al.*, Nature (London) **377**, 606 (1995).
[15] J. D. Kmetec *et al.*, Phys. Rev. Lett. **68**, 1527 (1992).
[16] M. Schnürer *et al.*, Phys. Plasmas **2**, 3106 (1995).
[17] K. Wharton *et al.*, APS Bull. **41**, 1465 (1996).
[18] A. P. Fews *et al.*, Phys. Rev. Lett. **73**, 1801 (1994); F. N. Beg *et al.*, Phys. Plasmas **4**, 447 (1997).
[19] C. K. Birdsall and A. B. Langdon, *Plasma Physics via Computer Simulations* (Adam Hilger, New York, 1991); J. Dawson, Phys. Plasmas **2**, 2189 (1995).
[20] A. Pukhov and J. Meyer-ter-Vehn, Phys. Rev. Lett. **76**, 3975 (1996).
[21] W. B. Mori *et al.*, Phys. Rev. Lett. **60**, 1298 (1988).
[22] E. Lefebvre and G. Bonnaud, Phys. Rev. Lett. **74**, 2002 (1995); Phys. Rev. E **55**, 1011 (1997).
[23] P. Gibbon and A. R. Bell, Phys. Rev. Lett. **68**, 1535 (1992).
[24] H. Ruhl and P. Mulser, Phys. Lett. A **205**, 388 (1995).
[25] C. Deutsch *et al.*, Phys. Rev. Lett. **77**, 2483 (1996).
[26] A. Pukhov and J. Meyer-ter-Vehn, APS Bull. **41**, 1502 (1996).
[27] G. A. Askar'yan *et al.*, JETP Lett. **60**, 251 (1994).
[28] S. V. Bulanov *et al.*, Phys. Lett. A **195**, 84 (1994).
[29] E. W. Weibel, Phys. Rev. Lett. **2**, 83 (1959); F. Pegoraro *et al.*, Phys. Scr. **T63**, 262 (1996).
[30] G. Shvets *et al.*, IEEE Trans Plasma Sci. **24**, 351 (1996).
[31] R. Lee and M. Lampe, Phys. Rev. Lett. **31**, 1390 (1973).
[32] H. M. Milchberg *et al.*, J. Opt. Soc. Am. B **12**, 731 (1995).
[33] F. Brunel, Phys. Rev. Lett. **59**, 52 (1987).